An alpaca nanobody neutralizes SARS-CoV-2 by blocking receptor interaction

Leo Hanke[1], Laura Vidakovics Perez[1], Daniel J Sheward[1,4], Hrishikesh Das[2], Tim Schulte[3], Ainhoa Moliner Morro[1], Martin Corcoran[1], Adnane Achour[3], Gunilla Karlsson Hedestam[1], B. Martin Hällberg[2], Ben Murrell[1*] and Gerald M McInerney[1*]

[1]Department of Microbiology, Tumor and Cell Biology, [2]Department of Cell and Molecular Biology and [3]Science for Life Laboratory, Department of Medicine Solna, Karolinska Institutet, and Division of Infectious Diseases, Karolinska University Hospital, Solna, Stockholm, Sweden. [4]Division of Virology, Institute of Infectious Diseases and Molecular Medicine, Faculty of Health Sciences, University of Cape Town, South Africa.

* These authors contributed equally.

For correspondence: Ben Murrell (benjamin.murrell@ki.se), Martin Hällberg (martin.hallberg@ki.se) and Gerald McInerney (gerald.mcinerney@ki.se).

Abstract

We report the isolation and characterization of an alpaca-derived, single domain antibody fragment (nanobody) that specifically targets the receptor binding domain (RBD) of the SARS-CoV-2 spike glycoprotein (spike) and potently neutralizes the virus. A cryo-electron microscopy structure of the bound complex at 2.9 Å resolution reveals that the nanobody (Ty1) binds to an epitope on the RBD accessible in both the 'up' and 'down' conformations and that Ty1 sterically hinders RBD-ACE2 binding. Mechanistic characterization confirms that Ty1 directly interferes with host cell receptor binding. This 12.8 kDa nanobody binds the SARS-CoV-2 spike with high specificity and affinity, and can be produced in high quantities recombinantly thereby offering potential as a potent and widely accessible SARS-CoV-2 antiviral agent.

Introduction

SARS-CoV-2 emerged as the etiologic agent of covid-19 in Wuhan, China in late 2019. In the comparatively short time since then, it has achieved pandemic status, causing more than 5.5 million cases, leading to at least 378,000 deaths and rising. Accordingly, the WHO declared the pandemic to be a public health emergency of international concern. A safe and effective vaccine is urgently needed, but requires time to develop. In the meantime, and indeed also in the post-vaccine era, highly specific and potent antiviral interventions are needed. Many generic or repurposed candidates are in trials, but so far results have been unremarkable. Since the virus is newly emerged, specifically designed drugs have not yet reached late phase trials. When available, specific antiviral drugs or antibody therapies will be used to protect individuals at risk and their widespread use will allow immunologically naïve populations to exit lockdowns more safely.

The virus is closely related to SARS-CoV-1, both being members of the lineage 2 betacoronaviruses. Cell entry of both viruses is achieved by first binding to the cell surface expressed receptor angiotensin-converting enzyme 2 (ACE2), followed by conformational changes in the viral spike glycoprotein trimer and subsequent membrane fusion. The affinity of SARS-CoV-2 receptor binding domain (RBD) for ACE2 is considerably higher than that for SARS-CoV-1 [1,2], supporting efficient cell entry and likely contributing to pathogenesis. The RBD is a globular domain situated on the distal surface of the spike protein. Two conformations have been observed in the stabilized trimer. Specifically, one conformation where one RBD is ACE2-accessible while two are not and one conformation where all three RBDs are down, i.e. receptor inaccessible [2,3]. As the receptor-engaging part of the spike, the RBD is an attractive target for coronavirus neutralization, and a number of conventional neutralizing monoclonal antibodies that target the RBD and block receptor binding have already been isolated from convalescent patients [4–6].

Camelid-derived single domain antibody fragments, also called VHHs or nanobodies, offer several advantages over conventional antibodies as candidates for specific therapies. Despite being approximately one tenth of the size of a conventional antibody, they retain specificity and affinity similar to conventional antibodies while being far easier to clone, express and manipulate. They are readily expressed in bacteria in large quantities and show high thermal stability and solubility, making them easily scalable and extremely cost effective. Their modularity means that they can be oligomerized to increase avidity or to increase serum half-life [7]. Critical to their use as antivirals in humans, they can easily be humanized with existing protocols [8]. Importantly, they have proven to be highly potent inhibitors of viral infections in vivo, particularly respiratory infections [9,10].

Here, we describe the isolation, evaluation and molecular determination of an alpaca-derived nanobody, Ty1, directed to the receptor-binding domain of the SARS-CoV-2 spike glycoprotein. We demonstrate that the monomeric 12.8 kDa Ty1 molecule potently neutralizes SARS-CoV-2 spike pseudovirus. The nanobody binds with high affinity to the RBD in a manner that occludes ACE2 interaction. We have also determined the mechanism of neutralization to be due to direct interference with RBD binding to ACE2. Altogether, these results highlight the great potential of Ty1 as a SARS-CoV-2 antiviral agent.

Results

Generation of SARS-CoV-2 RBD-specific nanobodies

We immunized one alpaca with SARS-CoV-2 S1-Fc and RBD in a 60-day immunization schedule. We generated a phage display library and performed two consecutive rounds of phage display, followed by an ELISA-based binding screen (Fig. 1A). We isolated one nanobody, Ty1, that binds specifically to the RBD of the SARS-CoV-2 spike glycoprotein. In parallel we performed next generation sequencing (NGS) on the baseline and post-enrichment libraries, and quantified variant frequency before and after each enrichment step. Ty1 exhibited the greatest fold-change in frequency among all nanobody variants, increasing over 10,000-fold from baseline to after the second enrichment round (Fig.1B). We report the amino acid sequence of Ty1 in Figure 1C.

Ty1 neutralizes SARS-CoV-2 spike pseudotyped viruses

To determine whether Ty1 neutralized SARS-CoV-2 we employed an *in vitro* neutralization assay using lentiviral particles pseudotyped with the SARS-CoV-2 spike protein. Ty1 neutralized

SARS-CoV-2 pseudotyped viruses at an IC_{50} of 0.77 µg/ml (54 nM) (Fig. 2A). No neutralization of a lentivirus pseudotyped with VSV-G by Ty1 was evident, and control nanobodies produced and purified in the same way, but specific for either influenza A virus nucleoprotein [11] or GFP [12], showed no evidence of neutralization of SARS-CoV-2 pseudotyped viruses.

Ty1 specifically recognizes the SARS-CoV-2 spike protein in transfected and infected cells

To confirm that Ty1 is directed against the SARS-CoV-2 spike protein, we characterized the specificity of Ty1 by flow cytometry. We site-specifically conjugated a fluorophore to the C-terminus of the Ty1 by means of a Sortase A reaction and copper-free click chemistry (Ty1-AS635P), and stained untransfected cells and cells transiently transfected with SARS-CoV-2 spike under permeabilizing conditions (Fig. 2B). While untransfected and unstained cells displayed similar signals, cells expressing the viral spike protein showed a strong shift in fluorescence intensity when stained with Ty1-AS635P. The apparent double peak likely reflected the varying efficiency of this transient transfection. To determine if the same probe can be exploited to recognize the viral spike protein in immunofluorescence, we infected Vero E6 cells with infectious SARS-CoV-2 at MOI 1 for 24 hours and stained the fixed and permeabilized cells with Ty1-AS635P and anti-dsRNA antibody (Fig. 2C). While uninfected cells showed no signal, infected cells were strongly labelled with both dsRNA antibody and Ty1-AS635P. Thus, Ty1 recognized the viral spike glycoprotein with high specificity in its native conformation in SARS-CoV-2-infected cells. Importantly, the low background in both experiments also suggested that Ty1 is a highly specific and suitable tool for research, diagnostics and therapy.

Ty1 competes directly with ACE2 for binding to the RBD of SARS-CoV-2 spike

To understand the neutralizing activity, we evaluated the effect of Ty1 on RBD binding to ACE2. We site-specifically conjugated a fluorophore to the C-terminus of the RBD (RBD-AS635P) and used this probe to stain ACE2 expressing HEK293T cells (Fig. 2D). Preincubation of RBD-AS635P with unlabeled Ty1 resulted in a significant reduction of ACE2 staining, while preincubation with the control nanobody NP-VHH1 had no such effect. This result indicated that Ty1 directly prevents binding of SARS-CoV-2 RBD to its host cell receptor ACE2.

Ty1 binds the RBD with high affinity

The highly specific and high-affinity binding of Ty1 to the RBD was also confirmed in kinetic bio layer interferometry (BLI) experiments. Monomeric RBD bound to surface-immobilized Ty1, but not to NP-VHH1 or to biocytin-quenched Streptavidin (SAX) (Fig. 3A). Dipping of the two Ty1-sensors into RBD at a concentration of 550 nM yielded binding responses with fast association kinetics and amplitudes reaching 1.5 nm (red curves), while dipping of the two NP-VHH1-sensors into the same RBD solutions yielded responses comparable to the reference sensors (2x violet and blue as well as light-green curves, respectively). RBD did not bind to the SAX control (green curves). Approximately half of RBD remained bound to Ty1 after 45 min (2700 s) of dissociation.

Titration experiments performed under normal and high salt conditions revealed concentration-dependent kinetic response curves for binding of RBD to Ty1 (Fig. 3B). The derived semi-log concentration-response curves revealed sigmoidal line-shapes with fitted apparent K_D-values of 8 ± 1.5 and 13 ± 1.5 nm for binding at normal and high salt conditions, respectively.

Kinetic fits of each sensorgram applying a 1:1 binding model revealed reasonable fits for association phases of curves obtained at low and intermediate RBD concentrations, as well as for most dissociation curves (Fig. 3B and 3C, left panels). However, relatively large deviations of

the fits showed that the 1:1 interaction model did not fully explain the obtained data (residuals in Fig. 3C). Nevertheless, most of the single-sensorgram fits yielded K_D-values in the 10-100 nM range with association and dissociation constants of about 1-1.2 $*10^5$ $(Ms)^{-1}$ and 3.5–4.3$*10^{-3}$ s^{-1} (k_{on} versus K_D plot in the lower panel of Fig. 3B). Most protein-protein interactions have association rates in the 10^6 to 10^7 $M^{-1}s^{-1}$ range, therefore high-affinity interactions with K_D-values in the nM range have typically dissociation rates around $1*10^{-3}$ s^{-1} [13].

Altogether, we concluded from these results that RBD bound to surface-immobilized Ty1 with high affinity in the 5-50 nM range.

Cryo-EM of prefusion spike in complex with Ty1

To understand the structural basis underlying the potent neutralization of SARS-CoV-2 we performed a preliminary cryo-EM structure determination of the prefusion-stabilized spike ectodomain in complex with Ty1. The current cryo-EM reconstruction reaches an overall resolution of 2.9 Å (Fig. 4A; 0.143 FSC) with strong variation of estimated local resolution from high resolution in the core of the spike trimer to relatively low resolution in the top of the spike. Nevertheless, the current reconstruction clearly shows that the spike retains only one main conformation with one RBD ‘up’ and two RBDs ‘down’. Importantly, all three RBDs are decorated in their upper parts with a Ty1 nanobody. The nanobodies retain a similar binding orientation to the RBD whether the RBD is found in the ‘up’ or ‘down’ conformation (Fig. 4B,C). As ACE2 can only be bound by an RBD in the ‘up’ conformation, the current cryo-EM reconstruction clearly shows that ACE2 binding is sterically hindered from two sides (Fig. 4D). Specifically, ACE2 binding is blocked both by the Ty1 nanobody bound to the RBD in the ‘up’ conformation and the neighboring RBD in the ‘down’ conformation. Hence, ACE2 binding is sufficiently hindered with any two of the available three binding RBD sites in the spike trimer. As

177 the RBD-Ty1 interaction interface is poorly resolved in the present reconstruction, we currently
178 refrain from molecular modelling of the exact binding interactions.
179
180 **Discussion**
181
182 The current coronavirus pandemic has drastic consequences for the world's population, and
183 vaccines, antibodies or antivirals are urgently needed. Neutralizing antibodies can block virus
184 entry at an early step of infection and potentially protect individuals that are at high risk of
185 developing severe disease. We report the identification and characterization of a SARS-CoV-2
186 RBD-specific single domain antibody fragment (nanobody) termed Ty1 that potently neutralizes
187 the virus. We provide structural and mechanistic insights that demonstrate that Ty1 prevents
188 RBD binding to its host cell receptor ACE2, and thus prevents SARS-CoV-2 virions from
189 attaching to cells. Ty1 binds the RBD with a kD within the 5-50 nM range, and neutralizes
190 SARS-CoV-2 pseudotyped virus at an $IC_{50}$of 0.77ug/ml (54 nM), representing the most potent
191 SARS-CoV-2 specific nanobody reported to date.
192 We identified Ty1 by binding assay after consecutive rounds of phage display, simultaneously
193 monitoring sequence enrichment by NGS. Although Ty1 exhibited the greatest fold-enrichment
194 in the NGS analysis, multiple additional nanobodies exhibited enrichment of varying extent
195 across both rounds. As the correlation between phage display enrichment and neutralization is
196 likely imperfect, further analyses of our libraries will likely yield other potent SARS-CoV-2
197 neutralizing nanobodies. In addition to neutralization activity, we also show that Ty1 can be
198 used as a detection reagent in flow cytometry and immunofluorescence demonstrating its
199 suitability as a research tool and for diagnostics.
200 It should be noted that the nanobody Ty1 can be readily produced in bacteria at very high yield
201 (in excess of 30 mg/L culture), and shows high affinity, making it an excellent candidate as a
202 low-cost, scalable antiviral agent against SARS-CoV-2, and we provide the amino acid

sequence, encouraging direct exploitation as such. While a llama nanobody capable of binding SARS-CoV-2 has recently been isolated, this molecule was elicited against SARS-CoV-1 and Fc-fusion was required to mediate neutralization of SARS-CoV-2 [14], precluding expression in bacterial culture. Since Ty1 already neutralizes as a monomeric protein, the generation of homodimeric or trimeric fusion constructs is likely to further increase its neutralization activity. Our structural results provide a template for the rational design of such oligomers that will potentially 'lock' the spike in a receptor-inaccessible conformation. Based on our work, we hope that Ty1 can be investigated as a candidate for antiviral therapy.

Methods

Cells and virus

Vero E6 cells and HEK293T cells (ATCC-CRL-3216) were maintained in Dulbecco's Modified Eagle Medium (Gibco) supplemented with 10% fetal calf serum and 1% Penicillin-Streptomycin and cultured at 37°C in a humidified incubator with 5% CO_2. A HEK293T cell line engineered to overexpress human ACE2 (HEK293T-ACE2) was generated by the lentiviral transduction of HEK293T cells. Briefly, lentiviruses were produced by co-transfecting HEK293T cells with a plasmid encoding VSV-G (Addgene cat#12259), a lentiviral Gag-Pol packaging plasmid (Addgene cat#8455), and a human ACE2 transfer plasmid. Virions were harvested from the supernatant, filtered through 0.45 µm filters, and used to transduce HEK293T cells. All cell lines used for experiments were negative for *Mycoplasma* as determined by PCR.

Infectious SARS-CoV-2 [15] was propagated in Vero E6 cells and titrated by plaque assay.

Proteins and probes.

The plasmid for expression of the SARS-CoV-2 prefusion-stabilized spike ectodomain with a C-terminal T4 fibritin trimerization motif was obtained from [2]. The plasmid was used to transiently

transfect FreeStyle 293F cells using FreeStyle MAX reagent (Thermo Fisher Scientific). The S ectodomain was purified from filtered supernatant on Streptactin XT resin (IBA Lifesciences), followed by size-exclusion chromatography on a Superdex 200 in 5 mM Tris pH 8, 200 mM NaCl.

The RBD domain (RVQ – VNF) of SARS-CoV-2 was cloned upstream of an enterokinase cleavage site and a human FC. This plasmid was used to transiently transfect FreeStyle 293F cells using the FreeStyle MAX reagent. The RBD-FC fusion was purified from filtered supernatant on Protein G Sepharose (GE Healthcare). The protein was cleaved using bovine enterokinase (GenScript) leaving a FLAG-tag at the C-terminus of the RBD. Enzyme and FC-portion was removed on HIS-Pur Ni-NTA resin (Thermo Fisher Scientific) and Protein G sepharose (GE Healthcare) respectively, and the RBD was purified by size-exclusion chromatography on a Superdex 200 in 50 mM Tris pH 8, 200 mM NaCl.

In addition, the RBD domain (RVQ – VNF) was cloned upstream of a Sortase A recognition site (LPETG) and a 6xHIS tag, and expressed in 293F cells as described above. RBD-HIS was purified from filtered supernatant on His-Pur Ni-NTA resin, followed by size-exclusion chromatography on a Superdex 200.

The nanobodies were cloned for expression in the pHEN plasmid with a C-terminal Sortase recognition site (LPETG) and a 6xHIS tag. This plasmid was used to transform BL21 cells for periplasmic expression. Expression was induced with 1 mM IPTG at OD600 = 0.6; cells were grown overnight at 30°C. Nanobodies were retrieved from the periplasm by osmotic shock and purified by Ni-NTA affinity purification and size-exclusion chromatography.

Biotinylated and fluorescent probes were generated using Sortase A as described here [16] and here [17]. In brief, nanobodies were site-specifically biotinylated on the C-terminus using Sortase A 5M. Nanobody at a concentration of 50 μM was incubated with sortase A 5M (5 μM),

GGGK-biotin (200 µM) in 50 mM Tris, pH 7.5, 150 mM NaCl, 10 mM $CaCl_2$, for 2 hours at 25°C. Unreacted nanobody and sortase was removed with Ni-NTA resin and excess GGGK-biotin was removed with Zeba spin desalting columns (0.5 mL, 7k MWCO, Thermo Fisher Scientific).

To generate the fluorescently labeled probes, first a dibenzocyclooctyne-amine (DBCO-amine, Sigma Aldrich) was attached via sortase A to the nanobody or the RBD. (Reaction conditions: 50 µM RBD or nanobody, 50 µM Sortase A 5M, 8 mM DBCO-amine in 50 mM Tris pH 7.5, 150 mM NaCl, 10 mM $CaCl_2$, 2 hours, 25°C). Unreacted probe, sortase and excess DBCO-amine was removed using Ni-NTA resin and PD-10 columns (GE Healthcare) respectively. Abberior Star 635P-azide (Abberior GMBH) was attached to the DBCO-labeled proteins in a copper-free click chemistry reaction. Unreacted fluorophore was removed on PD-10 column (RBD) or size-exclusion chromatography (nanobody).

Alpaca immunization

Alpaca immunization and phage display was performed similarly as described here [18] and here [19]. In brief, the adult male alpaca Tyson at PreClinics, Germany, was immunized 4 times in a 60-day immunization schedule. SARS-CoV-2 S1-sheep-FC (Native Antigen Company, SKU: REC31806) was used for the first two immunization, and SARS-CoV-2 RBD produced in FreeStyle 293F cells was used for the last two immunizations.

Library generation and nanobody isolation

After the final boost, RNA was isolated from PBMCs (RNA Plus mini kit, Qiagen). For cDNA synthesis, SuperScript III RT (Thermo Fisher Scientific) was used with a combination of oligo(dT), random hexamers, or gene specific primers (AL.CH2, ATGGAGAGGACGTCCTTGGGT and AL.CH2.2 TTCGGGGGGAAGAYRAAGAC) [19].

Nanobody sequences were PCR amplified and cloned into a phagemid vector for expression as pIII fusion. This library was electroporated into TG1 cells (Lucigen).

Cells were inoculated with VCSM13 helper phage, and the resulting phage was enriched in two consecutive rounds of phage display on RBD immobilized on magnetic beads. After the second round of phage display, individual bacterial colonies were picked in a 96 well format, grown until OD = 0.6 and nanobody expression was induced by addition of 1 mM IPTG. After 16 hours incubation at 30°C, bacterial supernatant was used as primary detection reagent in an ELISA coated with RBD or S ectodomain. Bound nanobodies were detected with anti-E tag (Bethyl laboratories) secondary antibody. Positive clones were sequenced and cloned into the pHEN expression vector for further characterization.

Amino acid sequence of Ty1

MAQVQLVETGGGLVQPGGSLRLSCAASGFTFSSVYMNWVRQAPGKGPEWVSRISPNSGNIG
YTDSVKGRFTISRDNAKNTLYLQMNNLKPEDTALYYCAIGLNLSSSSVRGQGTQVTVSS

Next generation sequencing (NGS) and analysis of nanobody libraries.

Plasmids from nanobody libraries before enrichment, and after each enrichment step, were amplified for 13 cycles using Q5 High-Fidelity 2X Master Mix (NEB) according to manufacturer's instructions, using primers:
CACTCTTTCCCTACACGACGCTCTTCCGATCTCTCGCGGCCCAGCCGGCCATGG and
GGAGTTCAGACGTGTGCTCTTCCGATCTACCGGCGCACCACTAGTGCA, annealing at 72°C. Illumina indexing primers were added using an additional 9 cycles, with Kapa HiFi. Amplicons were size selected using Agencourt AMPure XP beads (bead ratio: 1:1), and were pooled at ratios of 6:2:1 for pre:post-1:post-2 libraries, to account for the reduction in diversity expected

during enrichment, and sequenced on an Illumina MiSeq using the MiSeq Reagent Kit v3 (2x300) MS-102-3003.

Paired-end reads were merged using USEARCH11 [20], and then processed in the Julia language, primarily using the NextGenSeqUtils.jl package [21]. Briefly, reads are trimmed of primer sequences, and deduplicated, maintaining read frequencies. Variant frequencies are calculated as combined frequency of any reads matching a variant within 3% nucleotide divergence, using a kmer-based distance approximation for rapid database search. Any reads with counts >3 from the second enrichment library are searched for their variant frequencies across all databases. When calculating enrichment, to avoid zeros due to sampling and to regularize against over-sensitivity to low-frequency baseline variants, all frequencies are increased by the reciprocal of the size of the pre-enrichment database.

Neutralization Assay

Pseudotyped viruses were generated by the co-transfection of HEK293T cells with plasmids encoding the SARS-CoV-2 spike protein harboring an 18 amino acid truncation of the cytoplasmic tail [22], a plasmid encoding firefly luciferase, and a lentiviral packaging plasmid (Addgene cat#8455) using Lipofectamine 3000 (Invitrogen). Media was changed 12-16 hours after transfection, and pseudotyped viruses were harvested at 48- and 72-hours post transfection, filtered through a 0.45 μm filter, and stored at -80°C until use. Pseudotyped neutralization assays were adapted from protocols previously validated to characterize the neutralization of HIV [23], but with the use of HEK293T-ACE2 cells. Briefly, pseudotyped viruses sufficient to generate ~100,000 RLUs were incubated with serial dilutions of nanobodies for 60 min at 37°C. Approximately 15,000 HEK293T-ACE2 cells were then added to each well and the plates were incubated at 37°C for 48 hours. Luminescence was then measured using Bright-Glo

(Promega) per the manufacturer's instructions on a GM-2000 luminometer (Promega) with an integration time of 0.3s.

Flow Cytometry

Cells were trypsinized and fixed in 4% formaldehyde/PBS and stained with RBD-AS635P under non-permeabilizing conditions or with Ty1-AS635P under permeabilizing conditions. Fluorescence was quantified using a BD FACSCelesta and the FlowJo software package.

Immunofluorescence

Vero E6 cells were seeded onto coverslips in a 24 well plate and incubated overnight at 37°C/5% CO_2. Cells were infected with SARS-CoV-2 at a MOI of 1 for 24 h. Cells were fixed with 4% (v/v) formaldehyde, permeabilized in 0.5% Triton X-100 and blocked in 5% horse serum. Cells were incubated with anti-dsRNA antibody (1:2000, J2 Scicons) for 1 hour at room temperature followed by 1 hour staining with the secondary antibody anti-mouse-Alexa488 (1:2000, Thermo Fisher Scientific), Hoechst (1:1000, Invitrogen) and Ty1-AS635P (0.05 µg/mL). Coverslips were mounted in mounting media and images were obtained using Zeiss Axiovert microscope and processed using Adobe Photoshop.

Biolayer interferometry (BLI)

BLI was performed using single-use high-precision streptavidin biosensors (SAX) on an eight-channel Octet RED instrument according to manufacturer's protocols (Fortebio)[24]. Assays were performed in 2xPBS comprising 0,05% Tween-20 (PBST). Biotinylated nanobodies Ty1 and NP-VHH1 were loaded at concentrations between 30 and 250 nM followed by quenching using biocytin to reach final sensor loads of between 0.15 and 0.7 nm.

For the comparative binding test, the eight sensors were divided into two sets, each comprising double sample as well as single reference and single control sensors. Sample and reference sensors were loaded with respective nanobodies. The SAX control was only quenched. Loading of the two sets was performed consecutively to reach similar immobilization levels, while subsequent association and dissociation phases were performed simultaneously. For association, the sample and control sensors were dipped into RBD, while the reference sensor was dipped into PBST. For titration experiments, all sensors were loaded simultaneously. During association one of the sensors was used as reference and only dipped into PBST.

Raw data were pre-processed, analyzed and fitted by applying the 1:1 binding model as implemented in the manufacturer's software[25] . The processed data were imported into Rstudio for visualization and further analysis [26–28]. The comparative binding test shown in Figure 3A comprises un-processed raw data. The titration data in Figure 3B were processed applying reference sensor subtraction and Savitzky-Golay filter operations. Raw data and the analysis visualization scripts will be uploaded to Dryad and/or Github.

Cryo-EM sample preparation and imaging

Spike trimer (0.7 mg/ml) and Ty1 (1.3 mg/ml) were mixed in a 1:8 molar ratio and incubated on ice for 5 minutes. A 3-µl aliquot of the sample solution was applied to glow-discharged CryoMatrix holey grids with amorphous alloy film (Zhenjiang Lehua Technology) in a Vitrobot Mk IV (Thermo Fisher Scientific) at 4 degrees and 100% humidity (blot 10 s, blot force 3).

Cryo-EM data collection was performed with EPU 2.7 (Thermo Fisher Scientific) using a Krios G3i transmission-electron microscope (Thermo Fisher Scientific) operated at 300 keV in the Karolinska Institutet 3D-EM facility. Images were acquired in nanoprobe EFTEM mode with a slit width of 10 eV using a GIF 967 energy filter (Ametek) and a K3 detector (Ametek) during 2.4 seconds with a dose rate of 4.1 e-/px/s resulting in a total dose of 38 $e^-/Å^2$ fractionated into 40

364 movie frames. Motion correction, CTF-estimation, fourier binning (to 1.02 Å/px), picking and
365 extraction were performed on the fly using Warp [29].
366 A total of 9,584 micrographs were and 350,022 particles were picked by Warp. Extracted particles
367 were imported into cryoSPARC v2.15.0 [30] for 2D classification, 3D classification and non-
368 uniform 3D refinement. The particles were processed with C1 symmetry throughout. After 2D
369 classification (300 classes) 219,491 particles were retained and used to build three ab-initio 3D
370 reconstructions. These were further processed for heterogenous refinement that resulted in one
371 reconstruction showing high-resolution structural features in the core of the spike. One round of
372 homogenous refinement followed by non-uniform refinement resulted in a final reconstruction to
373 an overall resolution of 2.9 Å (0.143 FSC) using 150,847 particles.
374
375 **Model building and structure refinement**
376 A structure of the 2019-nCoV spike protein trimer [14] (PDB: 6VSB) was used as a starting model
377 for model building. The model was extended and manually adjusted in COOT [31]. The Nanobody
378 structure was homology modelled using SWISS-MODEL [32] taking PDB:5JMR [33] as a
379 template. The missing regions of the RBD domains were built based on the RBD-Spike crystal
380 structure (PDB: 6LZG) [34]. Structure refinement and manual model building were performed
381 using COOT and PHENIX [35] in interspersed cycles with secondary structure and geometry
382 restrained. All structure figures and all EM density-map figures were generated with UCSF
383 ChimeraX [36].
384
385
386 **Acknowledgements**
387 SARS-CoV-2 virus was received from Jonas Klingström, KI. The authors thank James Voss
388 and Deli Huang for reagents. We thank PreClinics for their fast and efficient services and
389 Gunnar Schulte and Per-Åke Nygren for providing access to instruments for measuring binding

kinetics. We also thank Fondation Dormeur, Vaduz for generous support of flow cytometry equipment.This work was supported by an EU grant (CoroNAb) to BM, GM and GHK and by project grants from the Swedish Research Council to BM (2018-02381), BMH (2017-6702 and 2018-3808) and to GM (2018-03843).

The authors declare no conflict of interest

Bibliography

1. Shang J, Wan Y, Luo C, Ye G, Geng Q, Auerbach A, et al. Cell entry mechanisms of SARS-CoV-2. Proc Natl Acad Sci U S A. 2020;117: 11727–11734.

2. Wrapp D, Wang N, Corbett KS, Goldsmith JA, Hsieh C-L, Abiona O, et al. Cryo-EM structure of the 2019-nCoV spike in the prefusion conformation. Science. 2020;367: 1260–1263.

3. Walls AC, Park Y-J, Tortorici MA, Wall A, McGuire AT, Veesler D. Structure, Function, and Antigenicity of the SARS-CoV-2 Spike Glycoprotein. Cell. 2020;181: 281–292.e6.

4. Ju B, Zhang Q, Ge J, Wang R, Sun J, Ge X, et al. Human neutralizing antibodies elicited by SARS-CoV-2 infection. Nature. 2020. doi:10.1038/s41586-020-2380-z

5. Shi R, Shan C, Duan X, Chen Z, Liu P, Song J, et al. A human neutralizing antibody targets the receptor binding site of SARS-CoV-2. Nature. 2020. doi:10.1038/s41586-020-2381-y

6. Cao Y, Su B, Guo X, Sun W, Deng Y, Bao L, et al. Potent neutralizing antibodies against SARS-CoV-2 identified by high-throughput single-cell sequencing of convalescent patients' B cells. Cell. 2020. doi:10.1016/j.cell.2020.05.025

7. Bannas P, Hambach J, Koch-Nolte F. Nanobodies and Nanobody-Based Human Heavy

Chain Antibodies As Antitumor Therapeutics. Front Immunol. 2017;8: 1603.

8. Vincke C, Loris R, Saerens D, Martinez-Rodriguez S, Muyldermans S, Conrath K. General strategy to humanize a camelid single-domain antibody and identification of a universal humanized nanobody scaffold. J Biol Chem. 2009;284: 3273–3284.

9. Detalle L, Stohr T, Palomo C, Piedra PA, Gilbert BE, Mas V, et al. Generation and Characterization of ALX-0171, a Potent Novel Therapeutic Nanobody for the Treatment of Respiratory Syncytial Virus Infection. Antimicrob Agents Chemother. 2016;60: 6–13.

10. Cardoso FM, Ibañez LI, Van den Hoecke S, De Baets S, Smet A, Roose K, et al. Single-domain antibodies targeting neuraminidase protect against an H5N1 influenza virus challenge. J Virol. 2014;88: 8278–8296.

11. Hanke L, Knockenhauer KE, Brewer RC, van Diest E, Schmidt FI, Schwartz TU, et al. The Antiviral Mechanism of an Influenza A Virus Nucleoprotein-Specific Single-Domain Antibody Fragment. MBio. 2016;7. doi:10.1128/mBio.01569-16

12. Kirchhofer A, Helma J, Schmidthals K, Frauer C, Cui S, Karcher A, et al. Modulation of protein properties in living cells using nanobodies. Nat Struct Mol Biol. 2010;17: 133–138.

13. Pollard TD. A guide to simple and informative binding assays. Mol Biol Cell. 2010;21: 4061–4067.

14. Wrapp D, De Vlieger D, Corbett KS, Torres GM, Wang N, Van Breedam W, et al. Structural Basis for Potent Neutralization of Betacoronaviruses by Single-Domain Camelid Antibodies. Cell. 2020;181: 1004–1015.e15.

15. Monteil V, Kwon H, Prado P, Hagelkrüys A, Wimmer RA, Stahl M, et al. Inhibition of SARS-CoV-2 Infections in Engineered Human Tissues Using Clinical-Grade Soluble Human

435 ACE2. Cell. 2020;181: 905–913.e7.

436 16. Antos JM, Ingram J, Fang T, Pishesha N, Truttmann MC, Ploegh HL. Site-Specific Protein
437 Labeling via Sortase-Mediated Transpeptidation. Curr Protoc Protein Sci. 2017;89: 15.3.1–
438 15.3.19.

439 17. Witte MD, Theile CS, Wu T, Guimaraes CP, Blom AEM, Ploegh HL. Production of
440 unnaturally linked chimeric proteins using a combination of sortase-catalyzed
441 transpeptidation and click chemistry. Nat Protoc. 2013;8: 1808–1819.

442 18. Sosa BA, Demircioglu FE, Chen JZ, Ingram J, Ploegh HL, Schwartz TU. How lamina-
443 associated polypeptide 1 (LAP1) activates Torsin. Elife. 2014;3: e03239.

444 19. Alpaca (Lama pacos) as a convenient source of recombinant camelid heavy chain
445 antibodies (VHHs). J Immunol Methods. 2007;324: 13–25.

446 20. Edgar RC, Flyvbjerg H. Error filtering, pair assembly and error correction for next-
447 generation sequencing reads. Bioinformatics. 2015;31: 3476–3482.

448 21. Kumar V, Vollbrecht T, Chernyshev M, Mohan S, Hanst B, Bavafa N, et al. Long-read
449 amplicon denoising. Nucleic Acids Res. 2019;47: e104.

450 22. Rogers TF, Zhao F, Huang D, Beutler N, Burns A, He W-T, et al. Rapid isolation of potent
451 SARS-CoV-2 neutralizing antibodies and protection in a small animal model. bioRxiv. 2020.
452 p. 2020.05.11.088674. doi:10.1101/2020.05.11.088674

453 23. Sarzotti-Kelsoe M, Bailer RT, Turk E, Lin C-L, Bilska M, Greene KM, et al. Optimization and
454 validation of the TZM-bl assay for standardized assessments of neutralizing antibodies
455 against HIV-1. J Immunol Methods. 2014;409: 131–146.

456 24. Abdiche Y, Malashock D, Pinkerton A, Pons J. Determining kinetics and affinities of protein

457 interactions using a parallel real-time label-free biosensor, the Octet. Anal Biochem.
458 2008;377: 209–217.

459 25. Octet Systems Software \textbar ForteBio. Available:
460 https://www.fortebio.com/products/octet-systems-software

461 26. Wickham H. ggplot2: Elegant Graphics for Data Analysis. Springer; 2016.

462 27. Wickham H. tidyverse: Easily Install and Load the 'Tidyverse. R package version 1.2.1;
463 2017. Available: http://CRAN.R-project.org/package=tidyverse

464 28. Team RC. R: A language and environment for statistical computing. Vienna, Austria: R
465 Foundation for Statistical Computing; Available: http://www.R-project.org/

466 29. Tegunov D, Cramer P. Real-time cryo-electron microscopy data preprocessing with Warp.
467 Nat Methods. 2019;16: 1146–1152.

468 30. Punjani A, Rubinstein JL, Fleet DJ, Brubaker MA. cryoSPARC: algorithms for rapid
469 unsupervised cryo-EM structure determination. Nat Methods. 2017;14: 290–296.

470 31. Emsley P, Lohkamp B, Scott WG, Cowtan K. Features and development of Coot. Acta
471 Crystallogr D Biol Crystallogr. 2010;66: 486–501.

472 32. Waterhouse A, Bertoni M, Bienert S, Studer G, Tauriello G, Gumienny R, et al. SWISS-
473 MODEL: homology modelling of protein structures and complexes. Nucleic Acids Res.
474 2018;46: W296–W303.

475 33. Dahms SO, Creemers JWM, Schaub Y, Bourenkov GP, Zögg T, Brandstetter H, et al. The
476 structure of a furin-antibody complex explains non-competitive inhibition by steric exclusion
477 of substrate conformers. Sci Rep. 2016;6: 34303.

34. Wang Q, Zhang Y, Wu L, Niu S, Song C, Zhang Z, et al. Structural and Functional Basis of SARS-CoV-2 Entry by Using Human ACE2. Cell. 2020;181: 894–904.e9.

35. Adams PD, Afonine PV, Bunkóczi G, Chen VB, Davis IW, Echols N, et al. PHENIX: a comprehensive Python-based system for macromolecular structure solution. Acta Crystallogr D Biol Crystallogr. 2010;66: 213–221.

36. Goddard TD, Huang CC, Meng EC, Pettersen EF, Couch GS, Morris JH, et al. UCSF ChimeraX: Meeting modern challenges in visualization and analysis. Protein Sci. 2018;27: 14–25.

37. Myszka DG, Jonsen MD, Graves BJ. Equilibrium analysis of high affinity interactions using BIACORE. Anal Biochem. 1998;265: 326–330.

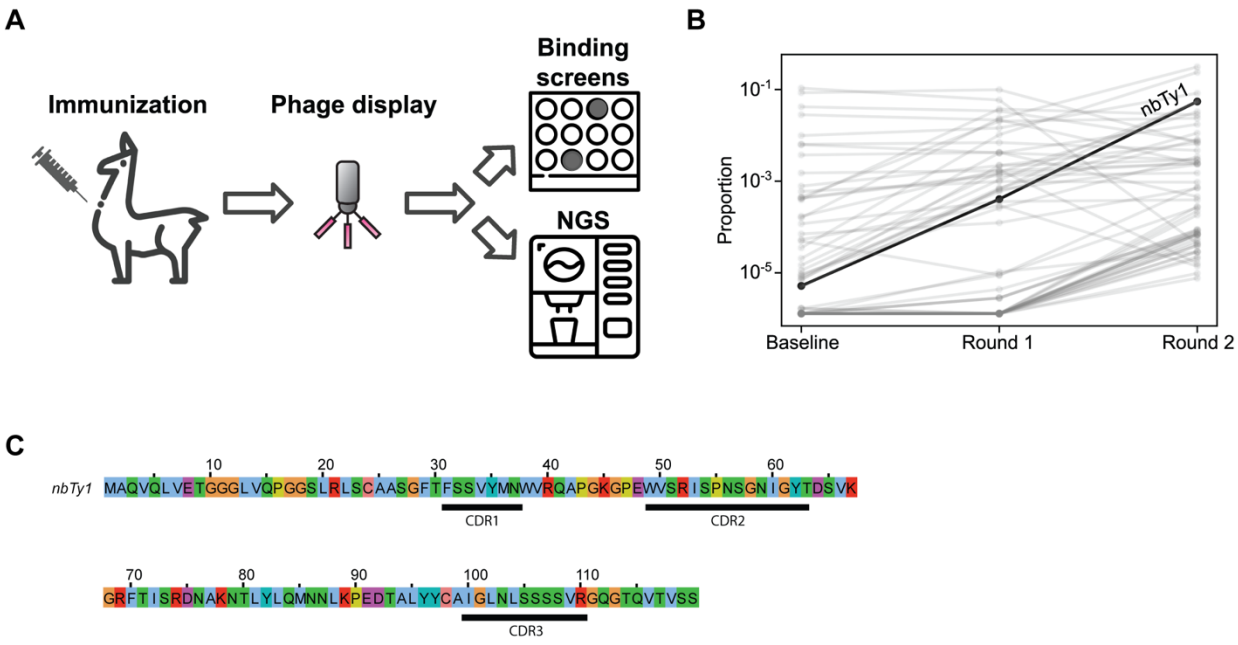

Figure 1 - Nanobody discovery.

A - Overview of nanobody generation process.

B - Variant frequencies quantified by NGS across successive enrichment steps. Identified using RBD bait, Ty1 exhibits the greatest total fold change of all nanobodies, increasing in proportion over 10,000-fold between initial and final libraries.

C - Sequence of Ty1. Complementarity-determining regions (CDRs) are indicated. Color scheme according to ClustalX.

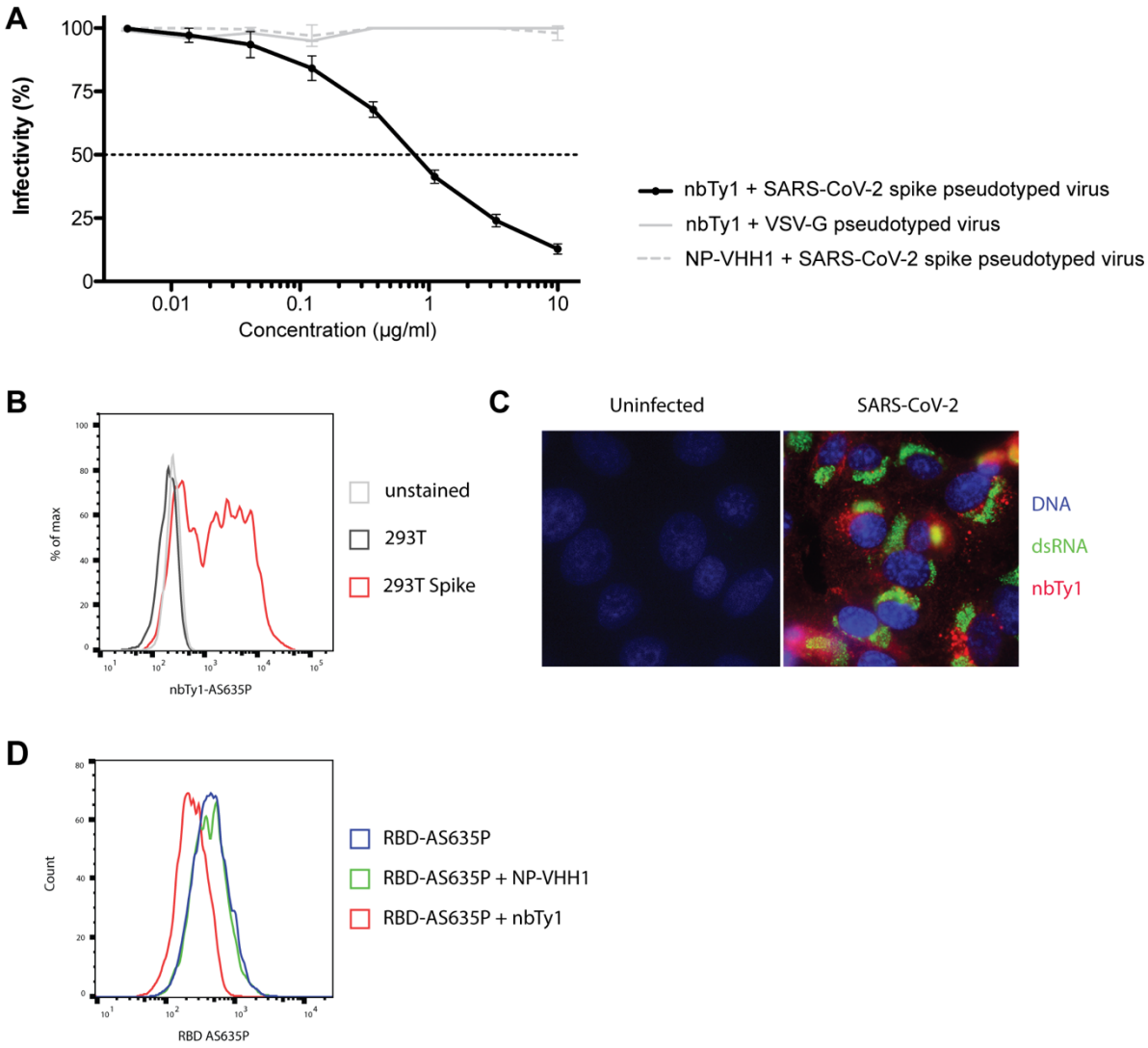

Figure 2 - Nanobody Ty1 neutralizes SARS-CoV-2 and specifically recognizes SARS-CoV-2 spike glycoprotein.

A - VSV G or SARS-CoV-2 spike pseudotyped lentivirus was incubated with a dilution series of Ty1 or control nanobody (influenza NP-VHH1 [11]). Infectivity relative to cells infected with pseudotyped virus in the absence of nanobody is shown. Neutralization by Ty1 was repeated in duplicate across 6 assays, and the error bars represent the standard deviation.

B - Cells were transfected with a plasmid harboring the SARS-CoV-2 spike for 24 h. Cells were fixed, permeabilized and stained with Ty1-AS635P (black and red) or left unstained (grey). Cells were analyzed by flow cytometry. Cell counts are presented as % of max (representative

histogram).

C - Vero E6 cells were infected with SARS-CoV-2 at a MOI of 1 for 24 hours. Cells were fixed, permeabilized and stained for DNA (blue), dsRNA (green) and with Ty1-AS635P (red). Pictures were taken by fluorescence microscopy and representative examples are shown.

D - ACE2 expression 293T cells were trypsinized, fixed and stained with RBD-AS635P alone, or preincubated with IAV NP-VHH1 or Ty1. Cells were analyzed by flow cytometry.

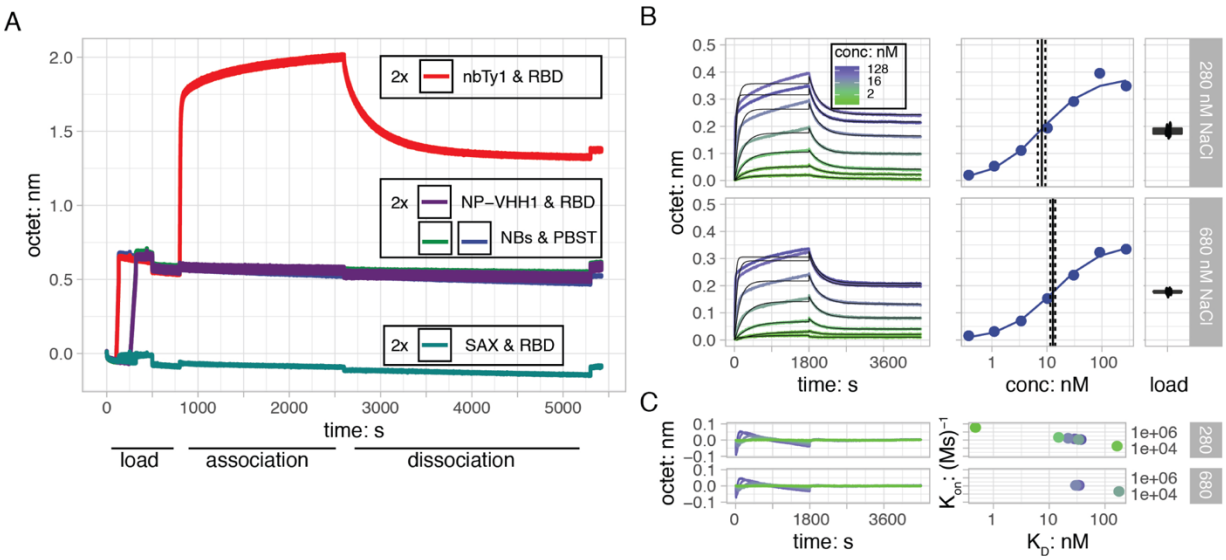

Figure 3 - RBD bound to surface-immobilized Ty1 with high affinity in the 5-50 nM range in Biolayer Interferometry

A - RBD bound to surface-immobilized Ty1 (red curves), but not to NP-VHH1 (violet curves) or to biocytin-quenched Streptavidin (SAX, green curves). Almost equal nanobody immobilization levels of about 0.7 nm were obtained by first loading Ty1 and then NP-VHH1. The SAX control surface (green) was quenched, but not loaded with nanobodies. During association, nanobody sample and control SAX sensors (red, violet and green) were dipped into RBD, while the reference nanobody sensors were dipped into PBST (blue and light-green). For dissociation, all sensors

were dipped into PBST. Binding of molecules over time is recorded as sensorgrams recording the shift in wavelengths (unit: nm) due to an increase in the optical thickness of the surface layer. B - *(left)* RBD titration sensorgrams reveal concentration-dependent responses with an association phase comprising a fast and a slow component. Dissociation seems to follow a single-exponential decay but does not return to baseline over the measurement time. Fitted 1:1 binding models are shown as thin lines. *(middle)* Pseudo-equilibrium response values extracted from the final association phase were plotted against the logarithmic Ty1 concentration. Single-site interaction fits of the sigmoidal binding curves according to [37] yielded K_D-values in the low nM range. K_D-values and standard deviations are shown as solid and dotted lines, respectively. *(right)* Sensor immobilization levels are shown as jittered box plots.

C - *(left)* Residuals of the 1:1 model fits to the interaction sensorgrams revealed that the simple 1:1 interaction model did not fully explain the obtained data, especially association phases at higher RBD concentrations. Color coding as in the sensorgram above. *(right)* Plot of fitted association rate constants (kon) versus affinity (K_D) values obtained from the kinetic 1:1 fits. Most of the fits grouped together at K_D values of 10-100 nM with association and dissociation constants of about 1-1.2 $*10^5$ $(Ms)^{-1}$ and 3.5–4.3$*10^{-3}$ s^{-1}, respectively.

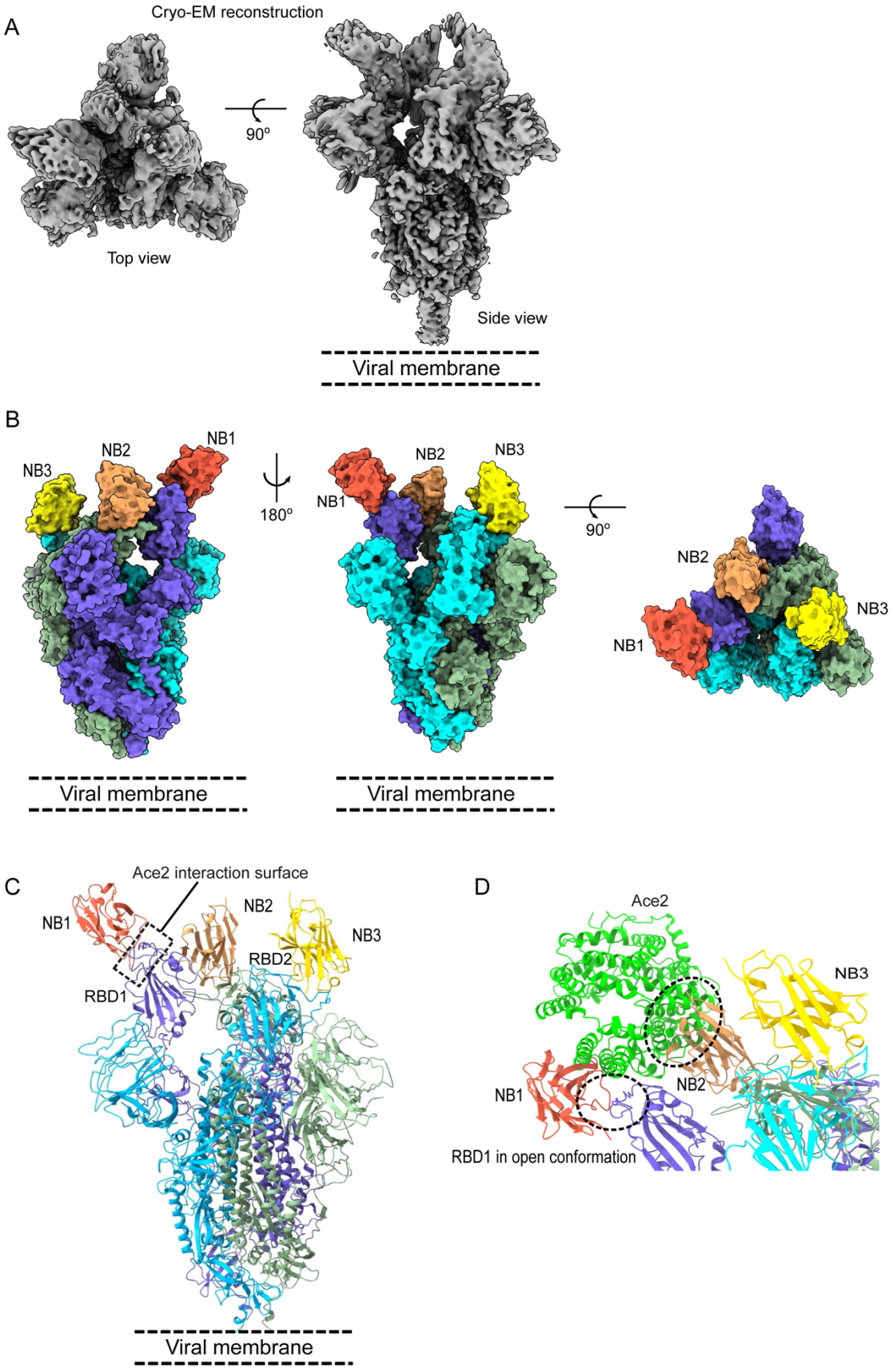

560

Figure 4 - Structure of the SARS-CoV-2 spike in perfusion conformation in complex with neutralizing nanobody Ty1

Ty1 binds to the RBD in 'up' and 'down' conformation and prevents ACE2 engagement

A - Cryo-EM reconstruction to an overall resolution of 2.9 Å of the spike trimer with bound Ty1

B - Surface representation of the spike trimer with three molecules of Ty1 bound. In our reconstruction, one RBD takes the 'up' and two RBDs have the 'down' conformation. Ty1 is bound on all three RBDs.

D - Cartoon representation of the spike trimer in complex with three molecules of Ty1.

E - Ty1 shows a two-pronged inhibition of ACE2 receptor binding through binding the RBD in the 'up' conformation and by binding to the neighboring RBD in the 'down' conformation.